npj | Quantum Materials

www.nature.com/npjquantmats

ARTICLE OPEN

Check for updates

Probing the interplay between lattice dynamics and short-range magnetic correlations in $CuGeO_3$ with femtosecond RIXS

E. Paris[1,7✉], C. W. Nicholson[2,7], S. Johnston[3], Y. Tseng[1], M. Rumo[2], G. Coslovich[4], S. Zohar[4], M. F. Lin[4], V. N. Strocov[1], R. Saint-Martin[5], A. Revcolevschi[5], A. Kemper[6], W. Schlotter[4], G. L. Dakovski[4], C. Monney[2] and T. Schmitt[1✉]

Investigations of magnetically ordered phases on the femtosecond timescale have provided significant insights into the influence of charge and lattice degrees of freedom on the magnetic sub-system. However, short-range magnetic correlations occurring in the absence of long-range order, for example in spin-frustrated systems, are inaccessible to many ultrafast techniques. Here, we show how time-resolved resonant inelastic X-ray scattering (trRIXS) is capable of probing such short-ranged magnetic dynamics in a charge-transfer insulator through the detection of a Zhang–Rice singlet exciton. Utilizing trRIXS measurements at the O *K*-edge, and in combination with model calculations, we probe the short-range spin correlations in the frustrated spin chain material $CuGeO_3$ following photo-excitation, revealing a strong coupling between the local lattice and spin sub-systems.

npj Quantum Materials (2021)6:51 ; https://doi.org/10.1038/s41535-021-00350-5

INTRODUCTION

Among the family of transition metal oxides, the charge-transfer materials are highly studied due to the realization of a number of exotic properties, from metal-insulator transitions to high-T_c superconductivity. These phenomena often arise from the microscopic coupling between charge, spin, orbital, and lattice degrees of freedom. In this regard, a significant advancement in understanding the origin of these exotic properties may be obtained by employing ultrafast time-resolved techniques to probe the dynamics of the relevant ordered phases. In the study of magnetism, the interplay between magnetic sub-lattices[1] and other degrees of freedom such as the crystal lattice[2–5] and charge[6–10], have afforded numerous important insights. However, when materials crystallize in a purely one-dimensional (1D) crystal structure they cannot support long-range magnetic order[11], even in the presence of strong short-range magnetic correlations. Such correlations are not easily accessible to many ultrafast techniques such as time-resolved photoemission, X-ray diffraction, or optical spectroscopies. In contrast, resonant inelastic X-ray scattering (RIXS) is able to probe both local magnetism and access elementary excitations rather than ordering phenomena[12–14]. Moreover, in contrast to most other local magnetic probes, the intrinsic timescale of the RIXS process (~1 fs) easily allows the extension of this technique to the ultrafast domain[15]. The main limitation for this class of experiments lies in the limited available time-integrated intensity. Indeed, only recently the progress of soft X-ray free-electron lasers (FELs) has allowed the very first few experiments of this kind[16–20]. The advent of the next-generation FELs worldwide is expected to overcome these limitations, enabling the study of a wide class of problems in condensed matter and beyond.

Using trRIXS therefore holds great promise for widening our understanding of ultrafast magnetism in low-dimensional and frustrated magnetic systems, allowing insights into their rich physics that include spin-glass phases, novel types of elementary excitations, and the fractionalization of quasi-particles. In this class of materials, the complexity of the phase diagrams often results from the competition between nearly degenerate ground states, and close competition between nearest neighbor (NN) and next-nearest neighbor (NNN) magnetic exchange coupling. A typical example of such physics is realized in the material $CuGeO_3$, whose structure is shown schematically in Fig. 1a. The basic building blocks of $CuGeO_3$ are CuO_4 plaquettes arranged in edge-shared chains running along the crystallographic *c*-axis[21]. The exchange interaction, *J*, between NN Cu ions depends on the interatomic distance and is antiferromagnetic (AFM), in large part due to a Cu–O–Cu bond angle of 99°[22]. The system is unstable towards a lattice dimerization, opening a spin-Peierls (SP) gap in the magnetic spectrum below a temperature $T_{SP} = 14$ K[23–26]. This process involves a magneto-elastic coupling between the 1D electronic system and the 3D phonon system. While the classical description of a SP transition holds only when the phonon energy is small compared to the other relevant energy scales, for $CuGeO_3$ the phonon energy scale is of the same order as the NN exchange coupling *J*[27]. The resulting entanglement of spin and lattice degrees of freedom is further complicated by the magnetic frustration induced by the presence of a large NNN AF exchange. In further contrast to typical SP materials such as TiOCl where the lattice dimerization is associated with the softening of a particular phonon mode[28,29], no soft phonon was ever observed in $CuGeO_3$. Even more remarkably, the two modes most strongly associated with the distortion are found to harden at low temperatures[30]. An additional quasi-elastic mode appears due to short-range fluctuations already well above the transition temperature[31] as evident in a number of experiments[32–34]. Therefore, due to the concomitant effect of low dimensionality and geometrical frustration, $CuGeO_3$ does not order magnetically over a long-range, and the physics is instead dominated by short-range magnetic correlations.

To obtain a better understanding of the intricate relation between spin and lattice degrees of freedom in this and other low-dimensional oxide materials, a direct measurement of the dynamics of short-range spin correlations is highly desirable. Here,

[1]Photon Science Division, Paul Scherrer Institut, Villigen PSI, Switzerland. [2]Département de Physique and Fribourg Centre for Nanomaterials, University of Fribourg, Fribourg, Switzerland. [3]Department of Physics and Astronomy, University of Tennessee, Knoxville, TN, USA. [4]Linac Coherent Light Source, SLAC National Accelerator Laboratory, Menlo Park, CA, USA. [5]SP2M, Institut de Chimie Moléculaire et des Matériaux d'Orsay, Université Paris-Saclay, CNRS, UMR 8182, 91405 Orsay Cedex, France. [6]Department of Physics, North Carolina State University, Raleigh, NC, USA. [7]These authors contributed equally: E. Paris, C. W. Nicholson. ✉email: eugenio.paris@psi.ch; thorsten.schmitt@psi.ch

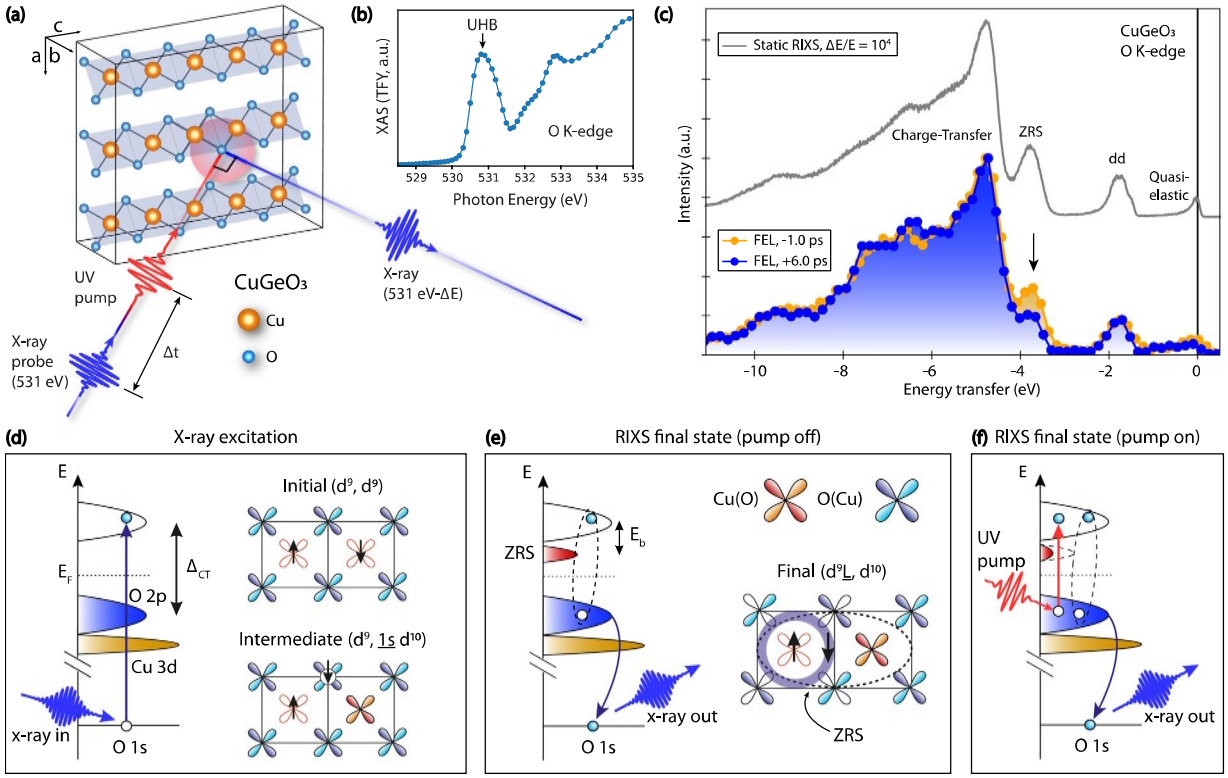

Fig. 1 Experimental overview and schematic of ZRS formation. a Sketch of the experimental scheme at the SXR beamline of the LCLS X-ray free-electron laser (FEL) facility. The laser pump pulse (4.7 eV, 50 fs) is followed by a collinear X-ray probe pulse (531 eV, 70 fs). The radiation re-emitted by the sample is then analyzed using a grating-based spectrometer. **b** Static O *K*-edge XAS spectrum of $CuGeO_3$, taken at 20 K using a synchrotron light source. The data are acquired in the same experimental geometry as the FEL experiment. **c** A comparison between the O *K*-edge RIXS spectrum obtained at a synchrotron radiation facility with a resolving power 10^4 (shown with a vertical offset) and those obtained with FEL radiation for a negative delay (yellow markers) and a positive delay (blue markers). Fluence = 37.4 mJ cm^{-2}. The black arrow marks the position of the Zhang–Rice singlet (ZRS) excitation. **d–f** Schematics of the ZRS formation in the O *K*-edge RIXS process described in the main text. In the schematics, E_F is the Fermi level, Δ_{CT} is the charge-transfer energy, and E_b is the ZRS binding energy.

we use time-resolved RIXS (trRIXS) to shed light on the interplay between lattice modulations, initiated by an ultrashort photo-excitation, and short-range magnetic correlations in a frustrated magnetic system. We employ 4.7 eV photons to excite the system across the charge-transfer gap, and O *K*-edge RIXS to track the photo-induced response of a Zhang–Rice singlet (ZRS) exciton, which is sensitive to the short-range spin correlations within the Cu–O chain of $CuGeO_3$[35]. Following photoexcitation, we observe an exponential decrease of the ZRS intensity, with some deviation caused by a partial recovery within ~1 ps, followed by a gradual reduction on longer time scales (10 ps), which persists to long delays (500 ps). This long-time effect increases linearly with the pump fluence up to a saturation above a critical value of 5 mJ cm^{-2}, which suggests the removal of a coupling channel between the magnetic and lattice sub-systems. Exact diagonalization calculations of the RIXS spectra at delays <10 ps imply the influence of a damped phonon which modulates the on-site Cu energy, therefore affecting the spin–spin correlation function. The timescale involved is compatible with a magneto-elastic mode at ~1 THz. In this way, we explore the effect of lattice dynamics on the short-range spin correlations in a frustrated low–dimensional spin system and set the stage for future investigations of these interactions exploiting next-generation X-ray FEL sources.

RESULTS

Zhang–Rice singlet detection with O *K*-edge RIXS

In our measurements, the energy of the FEL X-ray pulses is tuned to the O *K*-edge (~531 eV) and set to be resonant to an absorption peak sensitive to the upper Hubbard band (UHB) electrons[35]. The O *K*-edge XAS spectrum, collected with a synchrotron source, is presented in Fig. 1b. Fig. 1a shows the schematics of the trRIXS experiment: the pump and probe pulses propagate collinearly and impinge with an angle of 45° on the sample surface. In the experimental geometry, the CuO_4 plaquettes of copper–oxygen chains of $CuGeO_3$ lie at an angle of 56° with respect to the cleavage plane. The sample is kept at a temperature of 20 K during the measurements. Figure 1c displays a comparison between the O *K*-edge RIXS spectrum obtained in the trRIXS experiment (lower spectra) and a static high–resolution spectrum obtained under the same experimental conditions at a synchrotron source. Despite the lower statistics and energy resolution available in the FEL experiment, all of the main spectral components such as the quasi-elastic, d–d, and charge-transfer excitations are clearly visible. In particular, an excitation located at 3.8 eV[35] is well resolved and separated from the broad charge-transfer structure, located between 4–10 eV energy loss. Such excitation is due to the formation of a Zhang–Rice Singlet (ZRS) state.

In order to understand the relevance of the ZRS excitation for probing short-range spin correlations, we first clarify the mechanism of the ZRS formation in the RIXS experiment[35]. In the initial state (see Fig. 1d), the Cu ions in two neighboring CuO_4 plaquettes have a ($3d^9$, $3d^9$) orbital configuration, with a single hole in a hybridized Cu $3d_{x^2-y^2}$/O 2p orbital per plaquette. We assume an initial configuration with antiparallel spins. When an X-ray photon is absorbed, it promotes an electron from the oxygen 1s core level to fill a hole in the valence band and the plaquettes assume a (d^9, $d^{10}\underline{1s}$) configuration. From this excited state, a possible

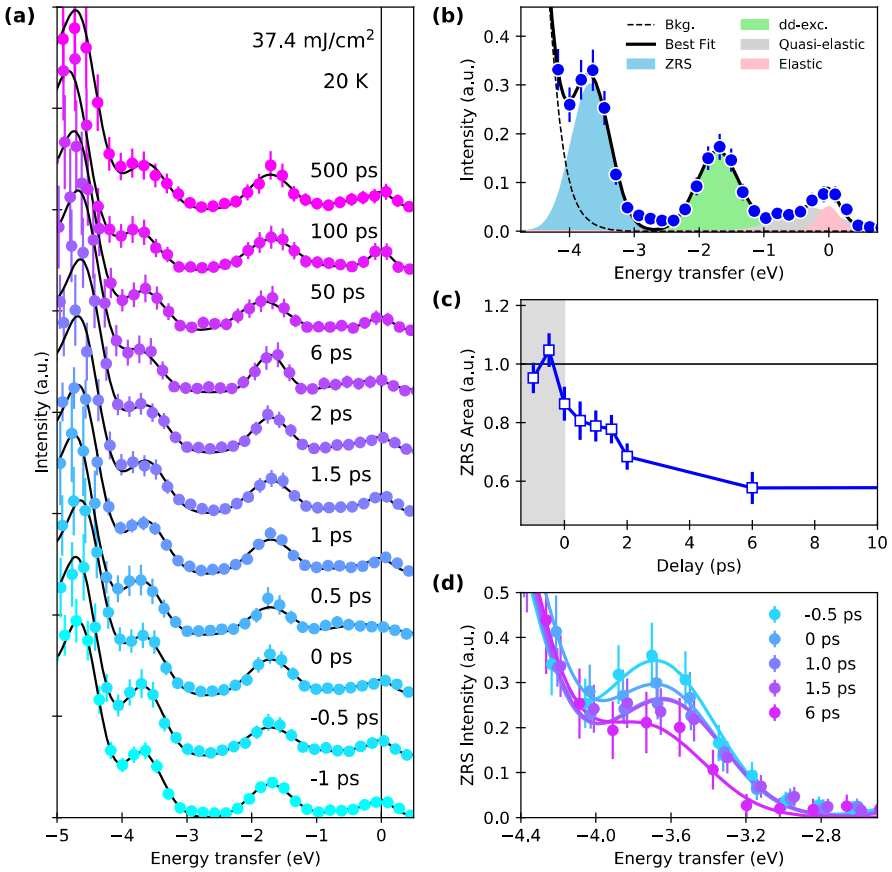

Fig. 2 Time-resolved RIXS spectra and ZRS dynamics. a O *K*-edge RIXS spectra (markers) collected with a pump fluence of 37.4 mJ cm^{-2}. Spectra taken at different pump-probe delays are shown with a vertical offset. The black line represents the best fit curve. The error bars are obtained by analyzing the fluctuation between different acquisitions taken under the same conditions. **b** Example of the multicomponent fit procedure used to extract the intensity of the ZRS excitation. The different components (denoted in the legend) are modeled with Gaussian functions. **c** Evolution of the integrated intensity of the ZRS excitation as a function of the pump–probe delay. The error bars represent the confidence interval obtained from the fit. **d** O *K*-edge RIXS spectrum around the ZRS excitation for selected time-delays as indicated in the legend.

de-excitation channel involves the relaxation of one ligand electron from the neighboring plaquette to fill the core-hole, leaving the system in a ($d^9\underline{L}$, d^{10}) configuration (see Fig. 1e). This mechanism involves a nonlocal charge transfer process, which is detected by the RIXS measurement[35,36]. In the RIXS final state, the two holes residing on the same plaquette inherit the initial antiparallel spin configuration and adopt the ZRS wave function. As a result of this bound ZRS exciton, the process gives rise to a peak at an energy transfer smaller than the charge gap (Δ) and separated from the continuum of charge-transfer excitations. It has been shown that the probability for such a process depends on the tendency of the neighboring Cu spins to be AFM oriented[35,37,38]. For this reason, the strength of the short-range AFM correlations is encoded in the spectral weight of the ZRS excitations probed by RIXS.

We excite the system across the charge-transfer gap using a 4.7 eV ultraviolet laser pulse. By comparing the O *K*-edge RIXS spectrum collected before (−1 ps) and after (+6 ps) the photo-excitation, presented in Fig. 1c, one can clearly identify a suppression in the intensity of the ZRS excitation as compared to the rest of the spectrum, which remains essentially unchanged.

Dynamics of the short-range antiferromagnetic correlations

Changing the pump-probe delay allows us to follow the development of the O *K*-edge trRIXS spectrum in the time domain. Although all the different excitations in the RIXS spectrum show some evolution following the arrival of the pump pulse, only the changes in the ZRS are clearly visible above the noise level. Therefore, in the following, we focus our analysis on the evolution of the ZRS intensity as a function of the pump–probe delay. Fig. 2a shows the O *K*-edge RIXS spectra between the elastic line and the charge transfer structure measured as a function of the time-delay for a laser fluence $F = 37.4$ mJ cm^{-2}. Such a high incident fluence is used due to the large penetration depth of photons at the pump wavelength[39,40] and corresponds to excitation of ~0.023 electrons per unit cell (see Supplementary Note 1, for the derivation of this value). The RIXS spectra in the region of the ZRS excitation are presented in Fig. 2d for selected time-delays. After 0.5 ps from the arrival of the pump pulse, we observe a rapid suppression of the ZRS intensity and partial recovery, as evidenced by a plateau in the dynamics (≈1 ps). This is followed by a further suppression which does not recover to the original intensity even after >100 ps (see Fig. 3d). By employing a multicomponent Gaussian fitting (as exemplified in Fig. 2b), we extract the dependence of the ZRS integrated intensity as a function of the time-delay, as shown in Fig. 2c, which confirms the dynamics already ascertained from the raw data. Directly after the laser excitation, we detect the fast suppression of the ZRS intensity with the additional plateau (~1 ps) followed by a longer reduction of intensity, saturating after ~10 ps. We note that the short time behavior depends strongly on the fitting model: in Supplementary Fig. 6c this plateau instead appears as a distinct peak, which we discuss further below. While the dynamics on the longer timescale

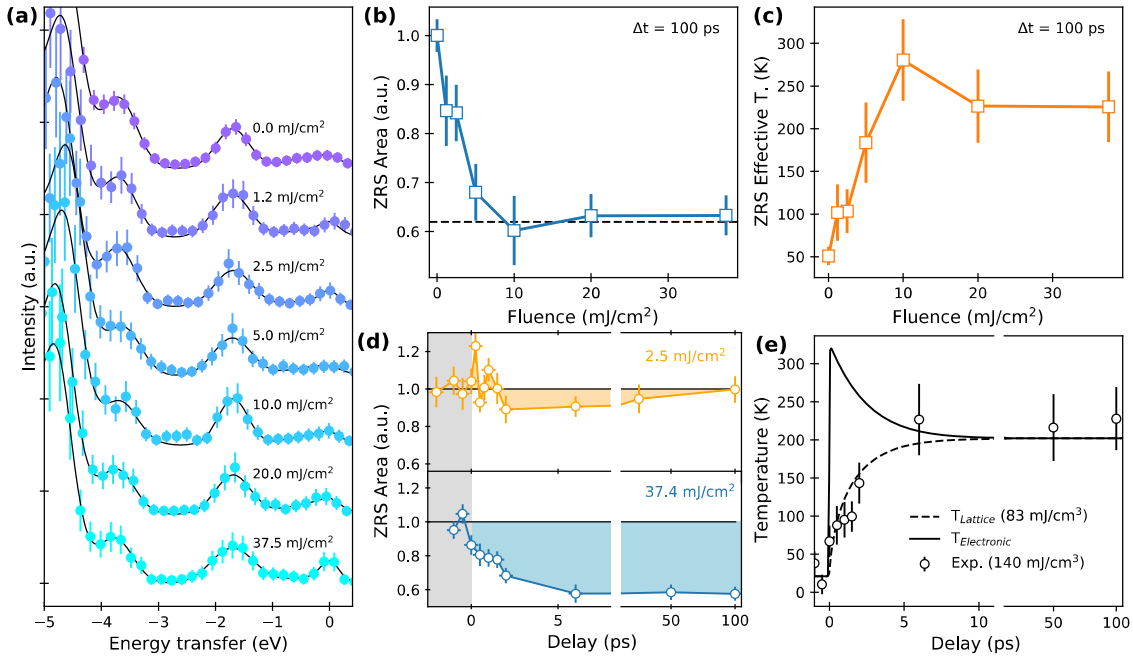

Fig. 3 Fluence dependent dynamics and effective temperature. a O *K*-edge RIXS spectra (markers) presented as a function of the pump fluence at $\Delta t = 100$ ps. Spectra are shown with a vertical offset for clarity. The black solid line represents the best fit curve. **b** Fluence dependence of the integrated intensity of the ZRS excitation, exhibiting saturation for $F > 5$ mJ cm^{-2} marked by the dashed line. The error bars represent the confidence interval from the least-square fit. **c** Fluence dependence of the effective ZRS temperature extrapolated using the static temperature dependence of the ZRS (see Supplementary Note 3). The saturation of the ZRS signal occurs below the room temperature value. **d** Time trace of the integrated intensity of the ZRS for two different laser fluences. Data are normalized to the average value at negative time-delays. Data at different fluence is shown with separated panels for clarity. **e** Two-temperature model describing the energy transfer between the electronic and lattice subsystems (see Supplementary Note 3). The solid line shows the electronic temperature, the dashed line the lattice temperature, while the white markers are experimental points. The absorbed heat content estimated for the experiment and the one used in the calculation are indicated in brackets in the legend.

are probably dominated by the quasi-thermal heating of the lattice, the short timescale plateau may have a nonthermal origin. In the following, we will address first the slow dynamics and then return to the origin of the rapid nonthermal behavior.

The time-dependent behavior up to long time-delays is presented in Fig. 3d for two different values of the laser fluence. The magnitude of the suppression of the ZRS peak intensity shows a large fluence dependence, being prominent at $F = 37.4$ mJ cm^{-2} and almost negligible at $F = 2.5$ mJ cm^{-2}. By fixing the time-delay at 100 ps, we have investigated the ZRS intensity for various pump excitation fluences, as presented in Fig. 3a. Using the fit procedure described before to extract the reduction of the ZRS reveals the onset of an abrupt saturation of the suppression for $F > 5$ mJ cm^{-2} (see Fig. 3b). Since these data are acquired at long delays, we initially assume that they predominantly reflect the reduction of the ZRS intensity caused by the increase in the thermal energy of the lattice at quasi-equilibrium with the spin and electronic systems. In the 1D crystal structure, the neighboring chains are decoupled, which results in inefficient heat transfer away from the probed volume into the crystal and may explain the observation that, even at very long delays, the ZRS intensity remains strongly depleted for high incident fluences. The long-time value of the ZRS intensity can be converted into an effective temperature by assuming a one-to-one correspondence with temperature-dependent static RIXS data (see Supplementary Note 3). The effective temperature reported as a function of the fluence in Fig. 3c, saturates at a value of ≈230 K. In contrast, the static temperature-dependent data only present a saturation behavior above room temperature (see Supplementary Fig. 7). Such a deviation from the equilibrium behavior is surprising as heat transport is likely to dominate on such long time scales, and at higher fluences more thermal energy is pumped into the system.

The same fitting analysis and comparison with static data can be applied to the transient ZRS behavior to extract the quasi-thermal evolution of the magnetic sub-system during the ultrafast measurements. The transient reduction of the ZRS peak as a function of time, again for $F = 37.4$ mJ cm^{-2} [Fig. 2c], is fitted with an exponential decay (see Supplementary Note 3). In order to gain further insight into these dynamics, we perform a commonly applied two-temperature model analysis. The model assumes that the electronic and lattice sub-systems are coupled heat baths that exchange energy following a pulsed excitation, which is captured by a system of two coupled differential equations (see Supplementary Note 3 for full details). The evolution of the electronic ($T_{\text{electronic}}$) and lattice temperature (T_{lattice}) can therefore be estimated from the electronic and lattice specific heats, and the amount of energy deposited by the laser pulse. The temporal evolution of the effective magnetic temperature can be quantitatively reproduced by this simple model, as shown in Fig. 3e, but only by assuming an absorbed heat content substantially lower than the amount estimated in the experiment. Indeed, by considering the mismatch in the penetration depth between the pump and the probe beams, for an incident laser fluence of 37.4 mJ cm^{-2} at the sample surface, we estimate an absorbed fluence of 140 mJ cm^{-3} within the volume probed by the X-rays (see Supplementary Note 1). However, using the estimated 140 mJ cm^{-3} as the input to the two-temperature model results in a dramatic overestimation of the rise in temperature when compared with that obtained from the ZRS intensity reduction. In fact, our model requires an input fluence of only 83 mJ cm^{-3} to describe correctly the experimental data. Thus, the magnetic system is cooler than expected as compared with a simple two-temperature analysis of the electronic and lattice systems. This discrepancy further implies that the ZRS selectively probes the

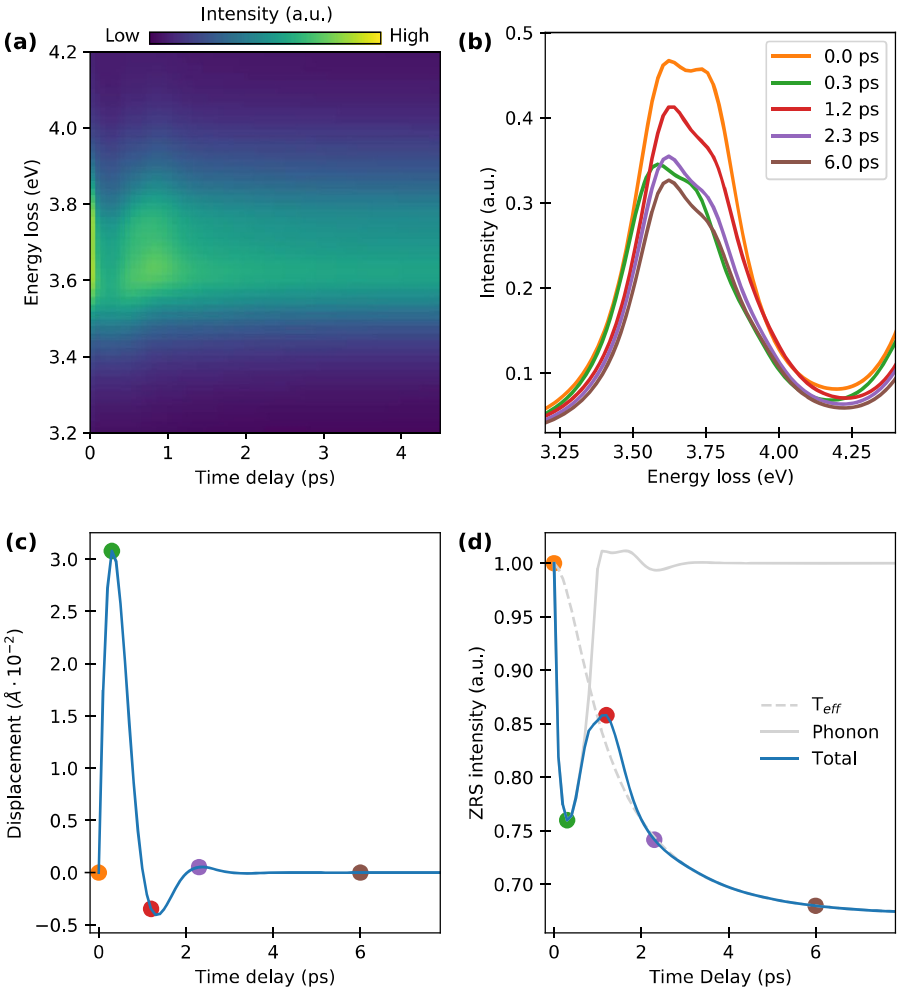

Fig. 4 Calculated trRIXS spectra in the region of the ZRS. a O *K*-edge RIXS in the vicinity of the ZRS excitation as a function of the time-delay, calculated using the Cu_3O_8 cluster model. **b** Calculated O *K*-edge RIXS spectra at selected time-delays. **c** Time evolution of the atomic displacement used in the calculation, including phenomenological exponential damping. **d** Computed time evolution of the ZRS intensity. The solid and dashed gray lines represent the effect of the lattice vibration and of the effective temperature on the computed ZRS intensity, respectively. The colored dots in the time traces of panels (**c**, **d**) represent time-delays chosen for the calculated RIXS spectra shown in panel (**b**), with the same color code. Full details of the calculations are provided in Supplementary Note 4.

dynamics of the magnetic sub-system, and that this becomes decoupled from the lattice and electronic systems in accordance with the fluence dependent results discussed above.

Nonthermal behavior at short timescales

A possible scenario resulting in the plateau in the otherwise exponential decrease of the ZRS spectral weight dynamics is a partial recovery caused by a damped coherent phonon oscillation, modulating the local magnetic correlations. Indeed, a large involvement of the lattice degrees of freedom was found in the transient response of $CuGeO_3$ following photoexcitation using optical techniques[41,42]. Even at equilibrium, the magnetic and lattice degrees of freedom are known to be strongly coupled in $CuGeO_3$. In particular, the bond angle between the Cu–O–Cu atoms of the plaquettes sensitively affects the AFM coupling strength. Even before the transition to the SP-phase, the lattice undergoes structural changes by compressing the plaquettes along the *a*-axis and extending them along the *c*-axis[22]. This compression further increases the Cu–O–Cu bond angle and, therefore, enhances the AFM correlations. Below T_{SP} an additional motion of the Ge side group is known to occur during the formation of the SP order[22,27,30], which also affects the AFM coupling.

In order to address whether a coherent phonon oscillation can lead to a modulation of the short-range magnetic order, we have utilized a cluster model of the plaquettes (ref. [35] and Supplementary Note 4). To capture the short-time dynamics of $CuGeO_3$, we introduced a coherent oscillation in our cluster, coupling linearly and uniformly to the charge transfer energy $\Delta = \varepsilon_p - \varepsilon_d$. We also introduced an effective temperature in our model, to capture the long-time dynamics. The RIXS spectra are then calculated at each time-delay using exact diagonalization and the Kramers–Heisenberg formalism (see further details in Supplementary Note 4). The results of this calculation in the region of the ZRS are presented in Fig. 4a with cuts at selected time-delays shown in Fig. 4b. Modulating the charge-transfer energy of the chains in the manner of a damped phonon oscillation, shown in Fig. 4c provides us with a possible explanation for the plateau at 1 ps in the observed fast dynamics of the ZRS intensity [Fig. 4d], namely the reduction and recovery after laser excitation. The slow reduction is also well reproduced by the effective temperature based on the experiment, as described above.

DISCUSSION

Our results reveal that the evolution of the magnetic degrees of freedom in $CuGeO_3$ decouple from the other degrees of freedom

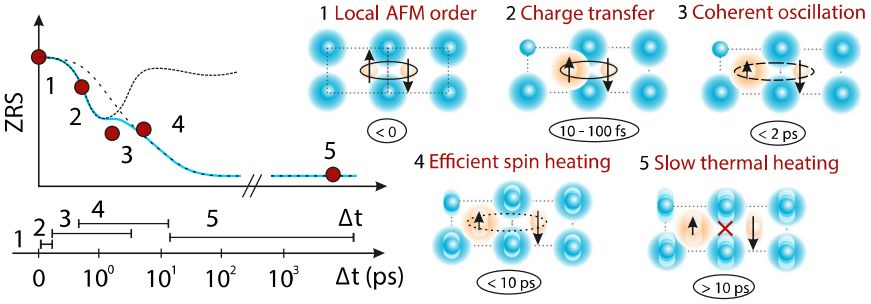

Fig. 5 Schematics of microscopic processes following photoexcitation. (Left) Approximate time scales for the different processes described (right). The pump pulse causes a charge transfer between O and Cu, which launches a short-range oscillation of a magneto-elastic mode, resulting in a modulation of the AFM coupling strength and correspondingly the ZRS intensity. Due to the heat transfer to the lattice, this mode is gradually removed, and therefore the lattice and magnetic temperatures separate.

on a 100 ps time scale and possibly follows a nonthermal behavior on the 1 ps time scale.

The observation of saturation of the ZRS intensity as a function of fluence at $\Delta t = 100$ ps (Fig. 3b) points towards the loss of an efficient coupling channel between the spin and phonon systems out-of-equilibrium. We note that while it is conceivable that this saturation could be caused by the suppression of the ZRS intensity due to the thermally heated lattice, such a scenario does not explain why the saturation occurs already at an equivalent temperature of ≈230 K, and not 300 K as observed in static RIXS (see Supplementary Fig. 7). This suggests a nonthermal behavior of the magnetic sub-system on a 100 ps timescale. Furthermore, it strongly implies the ZRS intensity is not a good measure of the quasi-equilibrium lattice temperature at all times, and can only reliably be used to probe the effective magnetic sub-system temperature. This conclusion is additionally supported by our two-temperature model, which requires a significantly lower input energy density than in the experiment to reproduce the observed magnetic temperature.

A potential origin for this loss of coupling between the two sub-systems is the removal of a low energy magneto-elastic mode at 0.9 THz observed in the SP-phase[43–49]. It has been suggested that this mode is a bound pair of magnons held together by the spin–phonon interaction[50,51] giving it a strong phononic component. Since this mode is gradually removed by the temperature at thermal equilibrium, it may also be quenched by the increased quasi-equilibrium temperature on the 10's of ps timescale.

Our model calculation reveals that a damped oscillation could be responsible for the observed nonthermal ultrafast dynamics of the ZRS. We emphasize that the plateau feature in our data depends strongly on the model used to fit the trRIXS spectra, and in particular whether the width of the ZRS is held constant or is left as a free fit parameter. In Supplementary Fig. 6c, we show that, in the latter case, the plateau is replaced by a clear peak in the time dynamics, with the ZRS width also changing rapidly after excitation. This gives further weight to the hypothesis that the plateau obtained in the more conservative analysis is indeed the result of a damped oscillation. However, there remains the possibility that a nonequilibrium state occurs where the ZRS is broadened nonthermally. Given the currently limited statistics, we leave this question open for future investigations. From the data in Fig. 2c, we can estimate an energy scale of ~4 meV (1 ps) from the frequency of this mode. There remains the question of exactly which atomic motion causes the change of the magnetic coupling. For the NN exchange in $CuGeO_3$, there are two significant factors that lead to an overall AFM nature of the coupling. The first is the fact that the Cu–O–Cu bond angle differs significantly from 90°, which removes the symmetry restriction on superexchange imposed by a 90° bond. The second is that the degeneracy of the O p_x and p_y orbitals is removed by the presence of a Ge sidegroup out of the plane of the CuO_4 plaquettes[22,52], allowing additional AFM coupling. Both the Cu–O and the Ge–O bonds change at the SP–distortion, and both may contribute to the modulation of the charge transfer energy (Δ), which equivalently modulates J. However, the frequencies of phonon modes most strongly associated with the motion of the Cu–O–Cu bond (3.3 and 6.8 THz)[30] and Ge bond (5–18 THz) are too large to account for the period of ≈1 ps (1 THz) that our data suggest. It is possible that the low energy mode at 0.9 THz discussed above may account for this behavior. To fully validate such a scenario will require further in-depth studies using next-generation X-ray FEL sources.

Based on our current findings we postulate the following speculative picture of the dynamics following excitation, as outlined in Fig. 5. Our measurements are performed at a temperature of 20 K. Although this temperature is higher than T_{SP}, short-range order fluctuations towards the spin-Peierls dimerization and concomitant singlet spin pairing are strong[32,33,53]. Within this environment, the intense ultraviolet pulse of 37.4 mJ cm^{-2} excites the electronic sub-system and creates a charge transfer from the O to the Cu ions. This leads to spatial redistribution of the electronic density in the CuO_2 chains of $CuGeO_3$ at 0 ps and acts as a trigger for launching a coherent oscillation with a period of < 2 ps, as observed in the spin response detected by RIXS via the ZRS excitation. We speculate here that this oscillation corresponds to the excitation of fluctuating magneto-elastic quasiparticles at very low energy. By modulating the bound magnon pairs via the spin–phonon coupling, this therefore results in a temporal modulation of the short-range AFM order, which is reflected in the ZRS intensity. Since the order is short-ranged, the coherent oscillation is strongly damped. At the same time, energy is efficiently transferred from the electronic into the lattice sub-system, raising the quasi-temperature of the lattice. As the quasi-temperature of the lattice increases, the magneto-elastic coupling gradually disappears. The rising lattice temperature has likely two consequences: (i) it contributes further to the damping of the coherent oscillation and (ii) the energy transfer into the magnetic sub-system becomes less efficient, because the suppression of the magneto-elastic quasi-particles closes a coupling channel between the two sub-systems.

Our time-resolved RIXS study uncovers intriguing physics in the nonequilibrium dynamics of a quasi-one-dimensional cuprate, $CuGeO_3$, allowing us to elaborate a possible scenario for their ultrafast evolution on the ps time scale. It calls for further experiments, with a more systematic approach regarding fluence and temperature dependences in particular. This will be made possible with next-generation X-ray free-electron facilities, allowing for higher statistics and for the acquisition of extensive data sets within a few days. In parallel, it would be important to reveal the ultrafast dynamics of the lattice degrees of freedom of $CuGeO_3$ directly. For instance, a future experiment using time-

resolved X-ray diffraction to monitor the structural distortion related to the spin-Peierls phase would be highly beneficial.

In summary, by allowing access to the short-range magnetic correlations in $CuGeO_3$, trRIXS provides us with a powerful tool to probe the ultrafast dynamics of the local spin arrangement. Our current study outlines the complex interplay between the electronic, lattice, and magnetic degrees of freedom in $CuGeO_3$. This establishes trRIXS as a technique capable of resolving the femtosecond dynamics of short-range magnetic correlations in low-dimensional and frustrated materials.

METHODS

Sample preparation and RIXS characterization

$CuGeO_3$ single crystals were cleaved at room pressure and temperature, producing mirror-like surfaces, and quickly transferred into the vacuum chamber (base pressure 10^{-9} mbar). The surface is oriented perpendicular to the [100] axis, so that the CuO_4 plaquettes are tilted 56° away from the surface. RIXS experiments were performed at the ADRESS beamline[54] of the Swiss Light Source, Paul Scherrer Institut, using the SAXES spectrometer[55]. A scattering angle of 90° was used and all the spectra were measured at the specular position, meaning that no light momentum is transferred to the system along the chain direction. The combined energy resolution was 60 meV at the oxygen K edge (~530 eV). Further details on the static RIXS measurements can be found in Supplementary Note 3.

Time-resolved RIXS (trRIXS)

Measurements were carried out at the SXR beamline of the Linac Coherent Light Source operating at 120 Hz[56]. The system is excited using a 4.7 eV ultraviolet laser pulse of 50 fs duration generated by frequency addition in nonlinear optical crystals. The energy of the 70-fs FEL X-ray pulses was tuned to the O *K*-edge (531 eV). The radiation scattered from the sample is collected by a compact spectrometer placed at a 90° scattering angle. The pump and probe pulses propagated collinearly and impinge with an angle of 45° on the sample surface. Both the laser pump pulse and the FEL probe pulse are horizontally polarized, i.e. the polarization vector lies in the scattering plane. In the experimental geometry, the CuO_4 plaquettes of copper–oxygen chains of $CuGeO_3$ lie at an angle of 56° with respect to the cleavage plane. The sample is kept at a temperature of 20 K during all the measurements. Further details on the trRIXS measurements can be found in Supplementary Note 1.

DATA AVAILABILITY

All the data used in the present manuscript are available on request. The data generated by our theory model can be found at https://github.com/JohnstonResearchGroup/Paris_etal_CuGeO3_2021.

CODE AVAILABILITY

The code used to perform the theory simulations can be found at https://github.com/JohnstonResearchGroup/Paris_etal_CuGeO3_2021.

Received: 6 August 2020; Accepted: 23 April 2021;
Published online: 21 May 2021

REFERENCES

1. Radu, I. et al. Transient ferromagnetic-like state mediating ultrafast reversal of antiferromagnetically coupled spins. *Nature* **472**, 205–208 (2011).
2. Vaterlaus, A., Beutler, T., Guarisco, D., Lutz, M. & Meier, F. Spin-lattice relaxation in ferromagnets studied by time-resolved spin-polarized photoemission. *Phys. Rev. B* **46**, 5280 (1992).
3. Stamm, C. et al. Femtosecond modification of electron localization and transfer of angular momentum in nickel. *Nat. Mater.* **6**, 740–743 (2007).
4. Wietstruk, M. et al. Hot-electron-driven enhancement of spin-lattice coupling in Gd and Tb 4f ferromagnets observed by femtosecond x-ray magnetic circular dichroism. *Phys. Rev. Lett.* **106**, 127401 (2011).
5. Maehrlein, S. F. et al. Dissecting spin-phonon equilibration in ferrimagnetic insulators by ultrafast lattice excitation. *Sci. Adv.* **4**, eaar5164 (2018).
6. Beaurepaire, E., Merle, J. C., Daunois, A. & Bigot, J. Y. Ultrafast spin dynamics in ferromagnetic nickel. *Phys. Rev. Lett.* **76**, 4250–4253 (1996).
7. Carley, R. et al. Femtosecond laser excitation drives ferromagnetic gadolinium out of magnetic equilibrium. *Phys. Rev. Lett.* **109**, 057401 (2012).
8. Nicholson, C. W. et al. Ultrafast spin density wave transition in chromium governed by thermalized electron gas. *Phys. Rev. Lett.* **117**, 136801 (2016).
9. Eich, S. et al. Band structure evolution during the ultrafast ferromagnetic-paramagnetic phase transition in cobalt. *Sci. Adv.* **3**, e1602094 (2017).
10. Tengdin, P. et al. Critical behavior within 20 fs drives the out-of-equilibrium laser-induced magnetic phase transition in nickel. *Sci. Adv.* **4**, eaap9744 (2018).
11. Mermin, N. D. & Wagner, H. Absence of ferromagnetism or antiferromagnetism in one- or two-dimensional isotropic Heisenberg models. *Phys. Rev. Lett.* **17**, 1133–1136 (1966).
12. Ament, L. J. P., Van Veenendaal, M., Devereaux, T. P., Hill, J. P. & Van Den Brink, J. Resonant inelastic x-ray scattering studies of elementary excitations. *Rev. Mod. Phys.* **83**, 705–767 (2011).
13. Schlappa, J. et al. Spin-orbital separation in the quasi-one-dimensional Mott insulator Sr_2CuO_3. *Nature* **485**, 82–85 (2012).
14. Le Tacon, M. et al. Intense paramagnon excitations in a large family of high-temperature superconductors. *Nat. Phys.* **7**, 725–730 (2011).
15. Wang, Y., Chen, Y., Jia, C., Moritz, B. & Devereaux, T. P. Time-resolved resonant inelastic x-ray scattering in a pumped Mott insulator. *Phys. Rev. B* **101**, 126–165 (2020).
16. Dean, M. P. M. et al. Ultrafast energy- and momentum-resolved dynamics of magnetic correlations in the photo-doped Mott insulator Sr_2IrO_4. *Nat. Mater.* **15**, 601–605 (2016).
17. Mitrano, M. et al. Ultrafast time-resolved x-ray scattering reveals diffusive charge order dynamics in $La_{2-x}Ba_xCuO_4$. *Sci. Adv.* **5**, eaax3346 (2019).
18. Wernet, P. et al. Orbital-specific mapping of the ligand exchange dynamics of $Fe(CO)_5$ in solution. *Nature* **520**, 78–81 (2015).
19. Parchenko, S. et al. Orbital dynamics during an ultrafast insulator to metal transition. *Phys. Rev. Res.* **2**, 23110 (2020).
20. Mitrano, M. & Wang, Y. Probing light-driven quantum materials with ultrafast resonant inelastic X-ray scattering. *Commun. Phys.* **3**, 184 (2020).
21. Völlenkle, H., Wittmann, A. & Nowotny, H. Zur Kristallstruktur von $CuGeO_3$. *Monatshefte Chem.* **98**, 1352–1357 (1967).
22. Braden, M. et al. Structural analysis of $CuGeO_3$: relation between nuclear structure and magnetic interaction. *Phys. Rev. B* **54**, 1105–1116 (1996).
23. Hase, M., Terasaki, I. & Uchinokura, K. Observation of the spin-Peierls transition in linear Cu^{2+} (spin-1/2) chains in an inorganic compound $CuGeO_3$. *Phys. Rev. Lett.* **70**, 3651–3654 (1993).
24. Hase, M. et al. Magnetic phase diagram of the spin-Peierls cuprate $CuGeO_3$. *Phys. Rev. B* **48**, 9616–9619 (1993).
25. Hirota, K. et al. Dimerization of $CuGeO_3$ in the spin-Peierls state. *Phys. Rev. Lett.* **73**, 736–739 (1994).
26. Castilla, G., Chakravarty, S. & Emery, V. J. Quantum magnetism of $CuGeO_3$. *Phys. Rev. Lett.* **75**, 1823–1826 (1995).
27. Braden, M., Reichardt, W., Hennion, B., Dhalenne, G. & Revcolevschi, A. Lattice dynamics of $CuGeO_3$: inelastic neutron scattering and model calculations. *Phys. Rev. B* **66**, 214417 (2002).
28. Seidel, A., Marianetti, C. A., Chou, F. C., Ceder, G. & Lee, P. A. S = 1/2 chains and spin-Peierls transition in TiOCl. *Phys. Rev. B* **67**, 20405 (2003).
29. Abel, E. T. et al. X-ray scattering study of the spin-Peierls transition and soft phonon behavior in TiOCl. *Phys. Rev. B* **76**, 214304 (2007).
30. Braden, M., Hennion, B., Reichardt, W., Dhalenne, G. & Revcolevschi, A. Spin-phonon coupling in $CuGeO_3$. *Phys. Rev. Lett.* **80**, 3634–3637 (1998).
31. Cowley, R. A. Structural phase transitions I. Landau theory. *Adv. Phys.* **29**, 1–110 (1980).
32. Chen, C. H. & Cheong, S.-W. Lattice fluctuations well above the spin-Peierls transition in the linear-chain system $CuGeO_3$. *Phys. Rev. B* **51**, 6777–6779 (1995).
33. Schoeffel, J. P., Pouget, J. P., Dhalenne, G. & Revcolevschi, A. Spin-Peierls lattice fluctuations of pure and Si- and Zn-substituted $CuGeO_3$. *Phys. Rev. B* **53**, 14971–14979 (1996).
34. Hirota, K. et al. Characterization of the structural and magnetic fluctuations near the spin-Peierls transition in $CuGeO_3$. *Phys. Rev. B* **52**, 15412–15419 (1995).
35. Monney, C. et al. Determining the short-range spin correlations in the spin-chain Li_2CuO_2 and $CuGeO_3$ compounds using resonant inelastic x-ray scattering. *Phys. Rev. Lett.* **110**, 087403 (2013).
36. Duda, L.-C. et al. Bandlike and excitonic states of oxygen in $CuGeO_3$: observation using polarized resonant soft-x-ray emission spectroscopy. *Phys. Rev. B* **61**, 4186–4189 (2000).
37. Monney, C. et al. Probing inter- and intrachain Zhang-Rice excitons in Li_2CuO_2 and determining their binding energy. *Phys. Rev. B* **94**, 165118 (2016).
38. Okada, K. & Kotani, A. Zhang-Rice singlet-state formation by oxygen 1s resonant x-ray emission in edge-sharing copper-oxide systems. *Phys. Rev. B* **63**, 045103 (2001).

39. Zagoulaev, S. & Tupitsyn, I. I. Electronic structure and magnetic properties of the spin-Peierls compound $CuGeO_3$. *Phys. Rev. B* **55**, 13528–13541 (1997).
40. Pagliara, S., Parmigiani, F., Galinetto, P., Revcolevschi, A. & Samoggia, G. Role of the Zhang-Rice-like exciton in optical absorption spectra of $CuGeO_3$ and $CuGe_{1-x}Si_xO_3$ single crystals. *Phys. Rev. B* **66**, 024518 (2002).
41. Giannetti, C. et al. Disentangling thermal and nonthermal excited states in a charge-transfer insulator by time- and frequency-resolved pump-probe spectroscopy. *Phys. Rev. B* **80**, 235129 (2009).
42. Marciniak, A. et al. Vibrational coherent control of localized d–d electronic excitation. *Nat. Phys.* **17**, 368–373 (2021).
43. Masayuki, U. et al. Raman scattering of $CuGeO_3$. *J. Phys. Soc. Jpn.* **63**, 4060–4064 (1994).
44. Kuroe, H. et al. Raman-scattering study of $CuGeO_3$ in the spin-Peierls phase. *Phys. Rev. B* **50**, 16468–16474 (1994).
45. van Loosdrecht, P. H. M., Boucher, J. P., Martinez, G., Dhalenne, G. & Revcolevschi, A. Inelastic light scattering from magnetic fluctuations in $CuGeO_3$. *Phys. Rev. Lett.* **76**, 311–314 (1996).
46. Muthukumar, V. N. et al. J1-J2 model revisited: phenomenology of $CuGeO_3$. *Phys. Rev. B* **55**, 5944–5952 (1997).
47. Loa, I., Gronemeyer, S., Thomsen, C. & Kremer, R. K. Spin gap and spin-phonon interaction in $CuGeO_3$. *Solid State Commun.* **99**, 231–235 (1996).
48. Kuroe, H. et al. Raman-scattering study of $CuGeO_3$. *Phys. B* **219–220**, 104–106 (1996).
49. Ogita, N. et al. Raman scattering of $CuGeO_3$. *Phys. B* **219–220**, 107–109 (1996).
50. Els, G. et al. Observation of three-magnon light scattering in $CuGeO_3$. *Phys. Rev. Lett.* **79**, 5138–5141 (1997).
51. Uhrig, G. S. & Schulz, H. J. Magnetic excitation spectrum of dimerized antiferromagnetic chains. *Phys. Rev. B* **54**, R9624–R9627 (1996).
52. Geertsma, W. & Khomskii, D. Influence of side groups on 90° superexchange: a modification of the Goodenough-Kanamori-Anderson rules. *Phys. Rev. B* **54**, 3011–3014 (1996).
53. Holicki, M., Fehske, H. & Werner, R. Magnetoelastic excitations in spin-Peierls systems. *Phys. Rev. B* **63**, 174417 (2001).
54. Strocov, V. N. et al. High-resolution soft x-ray beamline ADRESS at the swiss light source for resonant inelastic x-ray scattering and angle-resolved photoelectron spectroscopies. *J. Synchrotron Radiat.* **17**, 631–643 (2010).
55. Ghiringhelli, G. et al. SAXES, a high resolution spectrometer for resonant x-ray emission in the 400-1600 eV energy range. *Rev. Sci. Instrum.* **77**, 113108 (2006).
56. Schlotter, W. F. et al. The soft x-ray instrument for materials studies at the linac coherent light source x-ray free-electron laser. *Rev. Sci. Instrum.* **83**, 043107 (2012).

ACKNOWLEDGEMENTS

The static synchrotron experiments have been performed at the ADRESS beamline of the Swiss Light Source at the Paul Scherrer Institut (PSI). Work at PSI was funded by the Swiss National Science Foundation through the Sinergia project "Mott Physics Beyond the Heisenberg (MPBH) model" (SNSF Research grant numbers CRSII2_141962 and CRSII2_160765). This project was also supported by the Swiss National Science Foundation (SNSF) Grant No. PP00P2_170597. S. J. acknowledges support from the National Science Foundation under Grant No. DMR-1842056. Use of the Linac Coherent Light Source (LCLS), SLAC National Accelerator Laboratory, is supported by the U.S. Department of Energy, Office of Science, Office of Basic Energy Sciences under Contract No. DE-AC02-76SF00515. A.F.K. acknowledges support from the National Science Foundation under Grant No. DMR-1752713.

AUTHOR CONTRIBUTIONS

G.D., C.M., and T.S. conceived the project and coordinated the project phases. E.P., C.W.N., Y.T., M.R., and T.S. performed the static RIXS experiments at SLS/PSI with the assistance of V.N.S.; R.S.-M., and A.R. synthesized the samples. E.P., C.W.N., Y.T., G.C., S.Z., M.F.L., W.S., G.D., C.M., and T.S. carried out the trRIXS experiments at LCLS/SLAC. E.P., C.W.N., S.Z., and C.M. analyzed the data in discussion with T.S.; A.K. and S.J. performed the theoretical simulations. E.P., C.W.N., C.M., and T.S. wrote the manuscript with input from all authors. E.P. and C.W.N. contributed equally to this work.

COMPETING INTERESTS

The authors declare no competing financial or non-financial interests.

ADDITIONAL INFORMATION

Supplementary information The online version contains supplementary material available at https://doi.org/10.1038/s41535-021-00350-5.

Correspondence and requests for materials should be addressed to E.P. or T.S.

Reprints and permission information is available at http://www.nature.com/reprints

Publisher's note Springer Nature remains neutral with regard to jurisdictional claims in published maps and institutional affiliations.